

Conjugate heat transfer analysis of the tip seal in the counter rotating low pressure turbine

W. WRÓBLEWSKI, K. BOCHON

*Institute of Power Engineering and Turbomachinery
Silesian University of Technology
Konarskiego 18, 44-100 Gliwice, Poland
e-mail: krzysztof.bochon@polsl.pl*

THE AIM OF THIS STUDY WAS TO EXAMINE the phenomena associated with leakage flow through the tip seal with honeycomb land and to perform conjugate heat transfer (CHT) analysis of the entire tip area of the blade including the part of casing with rotating cavity above the seal.

CFD analyses were performed using commercial software. For the complicated geometrical configuration of the seal region, a calculation model was proposed which enabled a satisfactory approach to flow and heat transfer phenomena. CHT analyses were performed for two cases characterized by different thermal conductivity of the metal. Fluid flow parameters which allowed to recognize flow structures, losses and mixing were taken into account. In CHT analyses, the flow structures for the cavity, the heat transfer conditions as well as the temperature distribution in the whole domain were obtained.

Key words: CFD, tip seal, honeycomb, conjugate heat transfer.

Copyright © 2015 by IPPT PAN

Notations

b	cavity width, m,
c	specific heat for solid, J/(kg · K),
c_p	specific heat at constant pressure, J/(kg · K),
n	rotational speed, rpm,
Nu	Nusselt number,
q	heat flux,
T	temperature, K,
Tu	turbulence intensity,
v	velocity, m/s,
v_{ax}	velocity axial component, m/s,
v_t	velocity circumferential component, m/s,
y^+	dimensionless distance from the wall,
α	angle, °,
α	heat transfer coefficient, W/(m ² · K),
λ	thermal conductivity, W/(m · K),
ρ	density, kg/m ³ .

1. Introduction

TO ENSURE RELIABLE OPERATION OF THE TURBINE, adequate clearances should be retained between the rotating elements. The larger are the clearances, the greater the leakage flow and, consequently, the higher the energy losses. So, it is important to look for new solutions in seal designs which will allow for safe operation of the turbine with the least loss of energy.

The most common seals in steam and gas turbines are labyrinth seals, mainly because of their simplicity, low cost, reliability, flexibility of material selection, lack of pressure limitations and good tolerance to thermal variations. They are often combined with honeycomb land.

Labyrinth seals were studied in many instances. An example of a general assessment of the impact of leakage on turbine performance is presented by CHERRY *et al.* in [1]. The efficiency of the analysed turbine, after taking into account gaps and seals, decreased by 0.6% in comparison with the simplified case. Much attention was also paid to the evaluation of an impact of seals configuration on the leakage and modifications of seals to reduce leakage, see, for example, [2].

Leakage flux, which bypasses the blade-to-blade channel and does not perform work at this point, has the biggest impact on losses generated by the seal. But this is not the only factor that causes the loss in the seal. ROSIC and DENTON [3] estimated the impact of different mechanisms of loss generated the shroud leakage flows which consequently affect turbine performance. Besides the leakage flux, which bypasses the blade-to-blade channel, a great impact on losses generation has the process of mixing the re-entering leakage flux with the main flow. The other loss-generating mechanisms are associated with the existence of the inlet and outlet cavity and the shroud windage. However, the contribution of each factor to the loss-generating process depends on the seal construction.

Interactions between the re-entering leakage and the main flow were widely analysed, e.g., in [3, 4]. Modifications of the seal to limit the influence of the re-entering leakage on the main flow were analysed in [3, 6, 7].

Nowadays, honeycomb seals play an important role in control of leakages. They are widely used in turbomachinery because of their many advantages. They can withstand hard working conditions at high temperatures and high speeds, while allowing for limited rubbing without the danger of damaging the seal [8]. Therefore, a significantly tighter seal clearance, which represents a leakage-reducing factor, can be realized [9].

Honeycomb seals were the subject of numerous studies. Numerical calculations play a major role in these studies. CHOI and RODE [10] used a 3D model replacing the honeycomb cells with circumferential grooves. Recent investigations have shown new possibilities for the flow structure's modelling. A complete

geometrical representation of honeycomb cells was considered by SOEMARWOTO *et al.* [11]. A 3D mesh with over 10 million cells was used in their study. Fine meshes of this kind, the ones that take into account the honeycomb structure, can sufficiently capture the important flow features with high gradients around the knife-edge and in the swirl regions. Complete geometrical representation of the honeycomb cells was also used by LI *et al.* [9]. They considered axial flow through the three knives configuration with stepped honeycomb land. The influence of pressure ratio and sealing clearance on the leakage flow rate was investigated. In case of non-rotating honeycomb labyrinth seal, the influence of free space in the honeycomb cell above the seal fin, resulting in an increased leakage flow rate, was observed. A similar leakage flow rate was obtained for rotating and non-rotating honeycomb labyrinth seals.

Moreover, examples of analyses of different configurations and modifications of labyrinth seals with honeycomb land aimed at improving their efficiency are described, e.g., in [12, 13, 14]. KANG *et al.* [13] noticed that honeycomb enlarged leakage flow rate for all the considered seal configurations and seal clearances, but the leakage flow rate decreased with decreasing clearance.

Despite the increased leakage flow rate for the labyrinth seal with honeycomb land, this solution is used more frequently, both in new designs and as a part of modernization process. This is mainly caused by the possibility of safe seal clearance reduction, which eventually allows to reduce the leakage flow rate.

Because of heat resistance and turbine life time, it is very important to assess the heat transfer conditions in sealing devices. In addition, it is necessary to determine the temperature distribution and heat-transfer-coefficients.

Based on differences between experiments and CHT analyses, BORN *et al.* [16] observed a considerable influence of the computational mesh on accuracy of the results. In the case of solid domains discretisation is not very important, but it is crucial in the fluid domain. It is very important in the near-wall discretization and especially in the flow field at positions of important flow forms. HE *et al.* [17] in turn, noticed that the low Reynolds $k-\omega$ turbulence model and SST turbulence model provide a much better accuracy of heat transfer computations in the labyrinth seal than the $k-\varepsilon$ turbulence model.

HE *et al.* [17] and WEINBERGER *et al.* [18] analysed the impact of honeycomb land on the heat transfer conditions of the seal. HE *et al.* [17] noticed that in comparison with the smooth labyrinth seal, honeycomb cells reduced the heat transfer from the hot gas to the stator solid. Moreover, in comparison with the smooth labyrinth seal, the presence of honeycomb cells significantly decreased the temperature gradient in the cooled stator (solid domain). Similarly, WEINBERGER *et al.* [18] noticed that the honeycombs caused a vast decrease in stator temperatures. Additionally, according to the stator temperatures, the temperature drop across the seal was smaller for a configuration with honeycombs than

for the one without. In addition, a broad assessment of the impact of seal and honeycomb sizes on the conditions of heat transfer was included in the paper.

The aim of the study presented in the current paper is to examine the phenomena connected with leakage flow through the tip seal and CHT analysis of the whole tip area of the blade including: seal area, rotating cavity above the seal, the tip part of the blade-to-blade channel and the solid domain. The analyses were performed using ANSYS CFX tools.

2. Geometry model definition and mesh

CFD analyses were performed using the commercial software ANSYS-CFX. The area of interest concerns the tip part of the low pressure turbine rotor blade of an aircraft engine. It is complex and large structure in relation to scales of phenomena that occur; therefore definition of the calculation domain and the mesh quality played a very important role. The model for CHT analysis consisted of four independent domains (Fig. 1b), three domains for the fluid, included the blade-to-blade domain, the seal domain and the domain of the drum cavity. The solid multicomponent domain is reduced to a single domain and the real shape is simplified (Fig. 1a) to reduce the number of computational meshes and domain interfaces.

Each domain involved in CHT analysis is defined by an individual pitch corresponding to the geometrical configuration and the periodicity of physical phenomena. The honeycomb with the sealing area (area marked in red in Fig. 1) is the most demanding region in the entire computational model. This is due

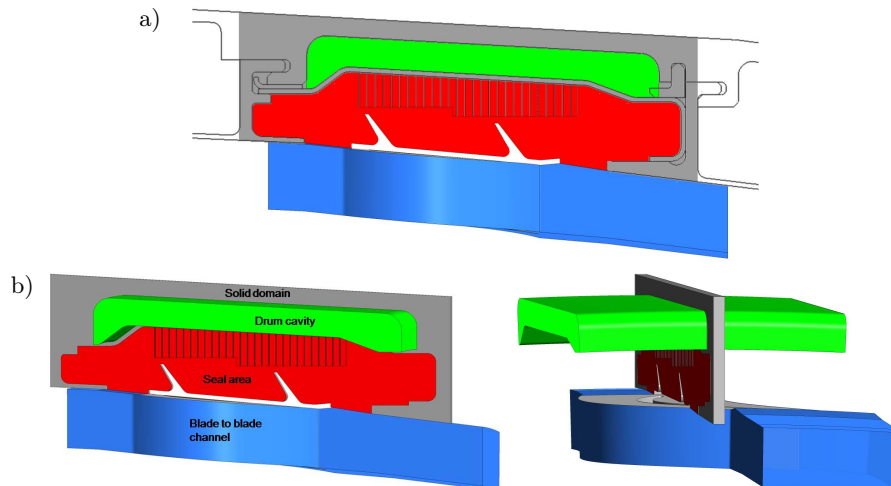


FIG. 1. Geometrical model for CHT analysis: a) solid shape simplification, b) definition of numerical domains.

to the small size of the honeycomb cells (1.5 mm), the size of metal sheets the honeycomb is made of, as well as to the size of fin tips and clearances above them, where, in addition, high flow velocity values and strong boundary effects can be observed. All this translates directly into large dimensions of the computational mesh. Therefore, a decision was made to limit this area as much as possible. In order to model the complete structure of the honeycomb, the circumferential size of the computational domain was limited to one full pitch of the honeycomb. Modelling the heat transfer in solids does not require significant expansion of the computational domain or a complex mesh, so the circumferential size was reduced to the smallest size of the flow domain, i.e., to the seal and the honeycomb area. In the case of the blade-to-blade channel, the standard approach was selected, in which the domain size was limited to the blade pitch.

In order to match the size of the drum cavity, preliminary calculations of the chamber were performed for three angles: 5, 15 and 45 degrees. The influence of the circumferential section size of the rotating cavity on the results was reported among others by SUN *et al.* [19]. Their analysis considered the flow structures and evaluated the impact of the domain size on the results. The calculations were performed for axial and radial temperature distributions on the chamber walls, in the range of 550–600 K. The aim was to simulate the effect of temperature drop in the stage as well as heating from the seal side and cooling from the outside. The results indicate that the flow phenomena that take place are not very intense and do not have a complex structure. Moreover, the relative velocity is low. It was also found that the model with the smallest angle (5°) adequately reflects the flow structures that are formed and essentially gives the same results as larger models. In addition, the mesh size for this model was small enough to be selected for further calculations. Further reduction in the domain size would limit the formation of flow periodic structures.

In previous stages of the calculations, not presented herein, seal optimization was carried out including an analysis of the mesh independent solutions [20]. For optimization purposes, a mesh was selected which was a compromise between the results' quality and the computation time. In order to improve the quality of results, the mesh for the seal area, which is the key element of the model, was thickened. For other areas, an adequate mesh was created. The computational mesh is presented in Fig. 2. The mesh for the blade-to-blade channel was generated as fully structural and consisted of about 2M nodes. For the remaining parts, the extruded hexa-dominant mesh was generated. The sizes of meshes for particular domains were as follows: for the seal domain – 4.4 M nodes, for the solid domain – 30 k nodes and for the cavity – 750 k nodes. The total number of nodes is about 7 M. All the meshes for fluid domains have y^+ values less than 2, but in the vast majority of the calculation area it was less than 1. Higher values occurred near the fin tips and on the bottom surface of the honeycomb land.

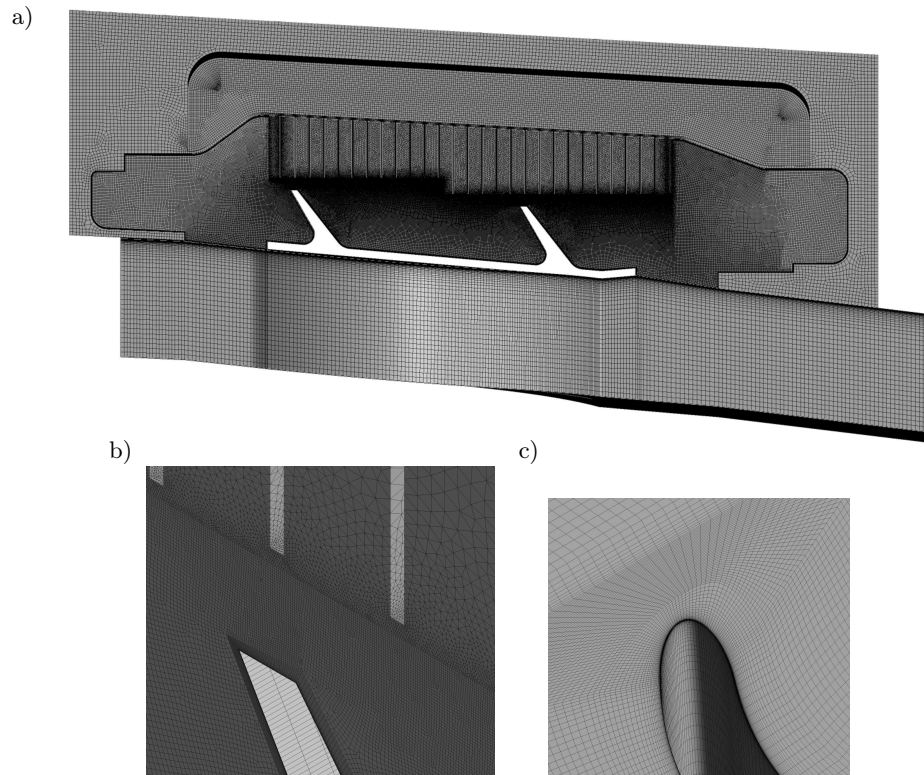


FIG. 2. Computational mesh: a) overall view, b) view of the mesh above the fin, c) mesh near the blade.

The relationships between individual domains are defined using appropriate fluid-fluid or fluid-solid interfaces. For the connection between the domain of the blade-to-blade channel and the seal domain, the fluid-fluid type interface was used with the frozen rotor option. In addition to this interface, the interfaces between the solid domain and domains for the blade-to-blade channel, the seal area and the drum cavity were defined. The solid domain and the cavity domain are rotating domains with the rotational speed of $n = -839$ rpm, like the seal domain. Consequently, the interface between the solid domain and the seal domain, whose pitches are the same, is defined without pitch change. The solid domain and the cavity domain have different pitches, and therefore the frozen rotor option had to be implemented for the interface.

3. Physical model and boundary conditions

Total pressure, total temperature and the flow angle distribution were applied at the inlet (Fig. 3) as functions of the blade height. Radial distribution of the

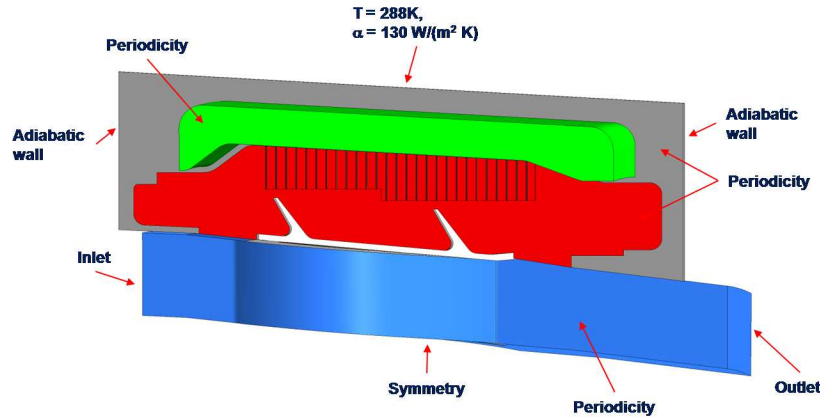


FIG. 3. Overview of boundary conditions for CHT analysis.

circumferentially averaged static pressure was used as a boundary condition at the outlet. Table 1 presents the average parameters in the main flow, which refer to the plane at the position of the blade trailing edge (TE) in the previous row, and the plane at the position of the blade leading edge (LE) in the next row. The parameters correspond to the results of the main flow path computations for the turbine, performed by Avio Aero. For the main flow at the inlet, the turbulence intensity Tu was assumed to be 5%.

The symmetry condition was used at the bottom wall of the channel. Periodic boundary conditions were applied to both sides of each calculation domain in order to take into account the 3D structure of the flow. The rotating speed of $n = 839$ rpm was applied to the blade-to-blade channel domain. The domain for the seal area rotated in the opposite direction at the rotating speed of $n = -839$ rpm.

Table 1. Main flow parameters applied to CFD model definition.

TE (previous row)					LE (next row)
Total pressure (absolute) [kPa]	Total temperature (absolute) [K]	$\alpha = \arctan(v_t/v_{ax})$ [°]	Static pressure [kPa]	Mach	Static pressure [kPa]
58.51	699.08	-62.74	55.28	0.291	51.55

All considered domains are periodic. The vertical surfaces of the solid domain are assumed as adiabatic walls. At the outer surface of the solid domain a forced convection is assumed with a bulk temperature $T = 288$ K, which corresponds

to ambient temperature at the ground level. The heat transfer coefficient was calculated using empirical correlations and its value was $\alpha = 130 \text{ W}/(\text{m}^2 \cdot \text{K})$.

The gas properties were set up as air ideal gas with the total energy heat transfer option. It means that the transport of enthalpy was modelled including kinetic energy effects. Molecular viscosity and conductivity were specified as a function of static temperature according to Sutherland's formula. The specific heat at constant pressure was specified as a function of temperature with the formula:

$$(3.1) \quad c_p = 0.0003T^2 - 0.1217T + 1014.4, \quad \text{J}/(\text{kg} \cdot \text{K}).$$

The drum material was assumed as stainless steel with constant density of $7900 \text{ kg}/\text{m}^3$ and specific heat of $585.2 \text{ J}/\text{kg}/\text{K}$. Two cases with different definitions of thermal conductivity λ are examined. In the first case – (Case I), the thermal conductivity is relatively low, and it is defined in [15] as

$$(3.2) \quad \lambda = 0.0182T + 6.13, \quad \text{W}/(\text{m} \cdot \text{K})$$

and in the second case – (Case II), the constant value $\lambda = 40 \text{ W}/(\text{m} \cdot \text{K})$ is set.

The first CHT calculations were made without taking into account the radiation. However, they have been repeated using the radiation model. This paper presents and compares the two cases. For radiation modeling, the P1 model was used. Unfortunately, more complex and more accurate models such as discrete transfer and Monte Carlo methods are not available in models consisting of computational domains with pitches. The applied model, however, allows to estimate the effects of radiation and its assessment in relation to other mechanisms of heat transfer.

The Grey spectral model was used in the calculations (all radiation quantities are uniform throughout the spectrum), the average emissivity for stainless steel was assumed as 0.4.

A high resolution advection scheme was set up for the continuity, energy and momentum equations. Similarly, the high resolution option was specified for the turbulence eddy frequency and the turbulence kinetic energy equations. Calculations were performed using the shear stress transport turbulence model with the Kato–Launder production limiter and the curvature correction.

4. Numerical analysis

The analysed tip seal with the honeycomb land is characterised by complex geometry and complex flow phenomena. The complex flow structures are characterised by high velocity flows over the fins, large velocity gradients, turbulence and intensive energy dissipation. The counter-rotating construction of the engine,

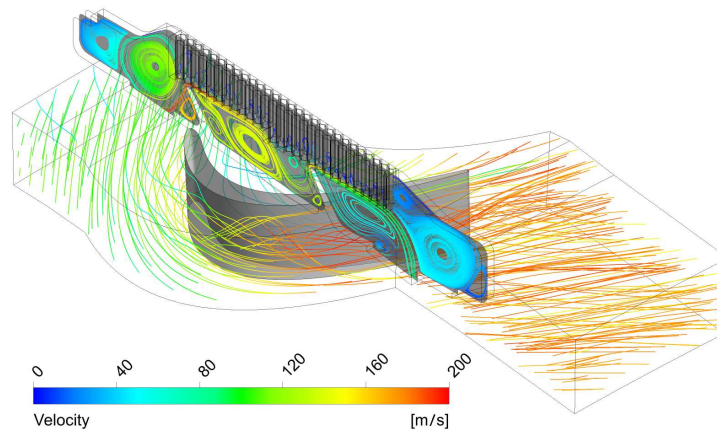


FIG. 4. Streamlines plot.

where the rotor and casing rotate in opposite directions, also plays an important role in modelling of the flow through the considered seal.

Figure 4 presents the streamlines plot for the analyzed geometry. They are the combination of three-dimensional streamlines in the blade-to-blade channel and surface streamlines in the seal area. The colour of the streamlines refers to the velocity in the relative frame of reference.

The leakage path in the seal area is relatively complex. The geometrical configuration of the seal favours the inflow of leakage flow at a sharp angle to the fins, what makes the contraction larger. Moreover, the significant curvature of the main path of leakage and nearly perpendicular inflow of the leakage on the honeycomb land causes the slowing down of the flow and leakage reduction.

Figure 5 presents the distribution of selected parameters along the leakage streamline. Because of losses in the seal, average values of the total pressure, static pressure and velocity are decreasing along the streamline, whilst the value of static entropy increases.

The total pressure as well as velocity is defined in a relative frame of reference. The static pressure, in particular cavities, does not change significantly. Its rapid decrease is observed on the seal fins, where the flow speeds up. In the cavity, the velocity of the leakage flow decreases.

The flow through the gaps above the fins, where significant contraction of the stream takes place, leads to the parameter fluctuations close to the honeycomb. This is visible on the charts, especially those of total pressure and static entropy. The fluctuations die away further in the flow. The phenomena can also be observed in Figs. 6–8, which present the distribution of total pressure, static entropy and turbulence kinetic energy in the seal area. The fluctuations are visible behind fins, close to the honeycomb.

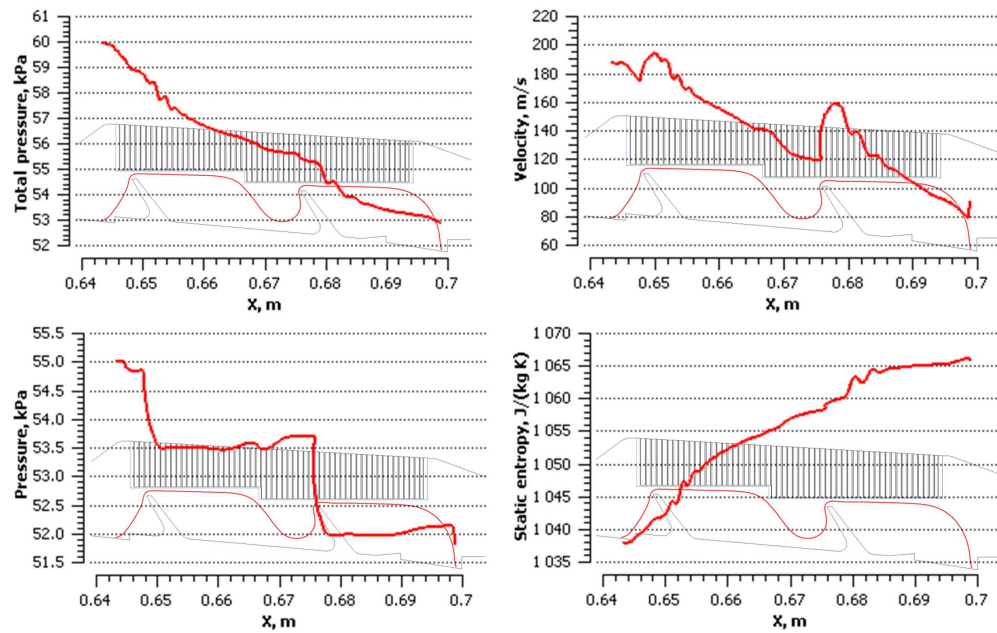


FIG. 5. Parameters distribution along the leakage streamline.

Figure 6 presents the total pressure distribution in the seal area. The leakage path through the seal is clearly visible. The total pressure drop along the leakage path, which is associated with the energy dissipation, can be also observed in Fig. 6 (as in Fig. 5). The largest drop is observed in the inlet chamber of the seal and behind the fins.

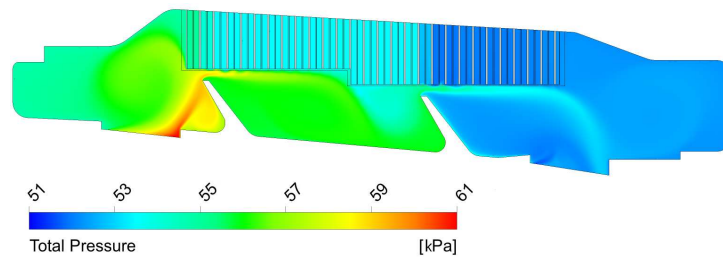


FIG. 6. Total pressure distribution in the tip seal.

The distribution of entropy in the calculation domain is shown in Fig. 7. The entropy distribution shows the places where losses are generated, e.g., due to turbulence. They are also visible in Fig. 8, where turbulence kinetic energy is

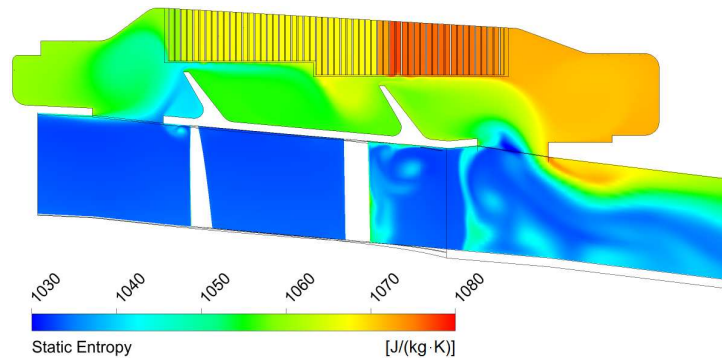


FIG. 7. Static entropy distribution in the tip seal.

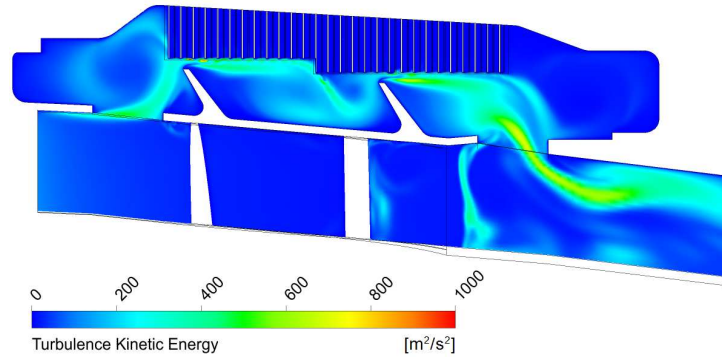


FIG. 8. Turbulence kinetic energy distribution in the tip seal.

presented. Besides losses in the seal, a small increase of entropy and turbulence kinetic energy can be observed in the main flow, behind the seal inlet, where a small vortex is formed. Large changes can be observed in the seal outlet area and behind the outlet, where the leakage interacts with the main flow.

An overview of the temperature distribution in the analysed area is presented in Fig. 9 for Case I and in Fig. 10 for Case II. The temperature distribution in the solid and the seal area is influenced by temperature distribution in the blade-to-blade channel and in the seal as well as by the assumed environment parameters and material properties of steel. Due to the lower value of thermal conductivity in Case I, we have to deal with lower temperatures in the upper part of the solid and with greater temperature gradient.

In the cavity above the seal, stratified temperature distribution can be observed, which is determined by the temperature difference between the seal area and the area outside the casing. Analysing Figs. 9 and 10 it can be concluded that the honeycomb plays an important role in the heat exchange between the

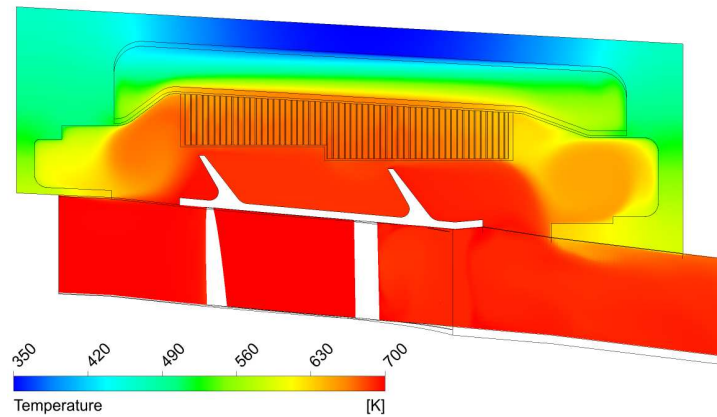


FIG. 9. Temperature contour from CHT results (Case I).

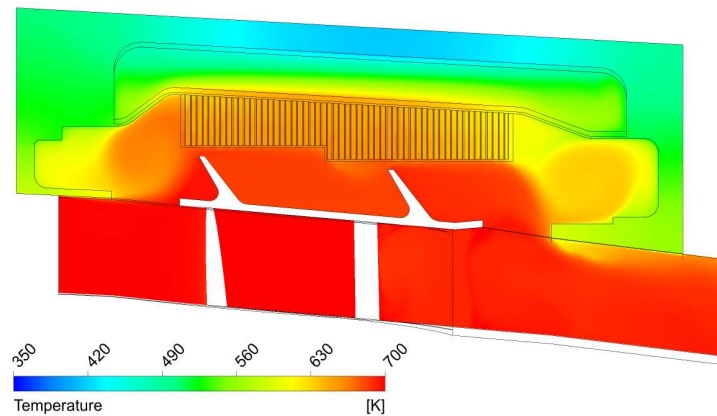


FIG. 10. Temperature contour from CHT results (Case II).

casing elements of the engine, the cavity and the seal. The largest temperature differences, resulting from different values of thermal conductivity, are observed in the region of honeycomb. Heat transfer in the honeycomb also causes the lower temperature level in the chamber located on the outlet of the seal, what is visible in Fig. 10. The temperature difference for Case I and II in the chamber above the inlet of the seal is less noticeable. Cooling of the solid domain by the outer region does not have a significant effect on the seal area.

Radiation affects the intensification of heat transfer in the upper part of the calculation area, resulting in an increase of temperature in the solid domain, the cavity above the seal and the chamber above the seal outlet. This effect, however, does not cause too much change in the pattern of temperature dis-

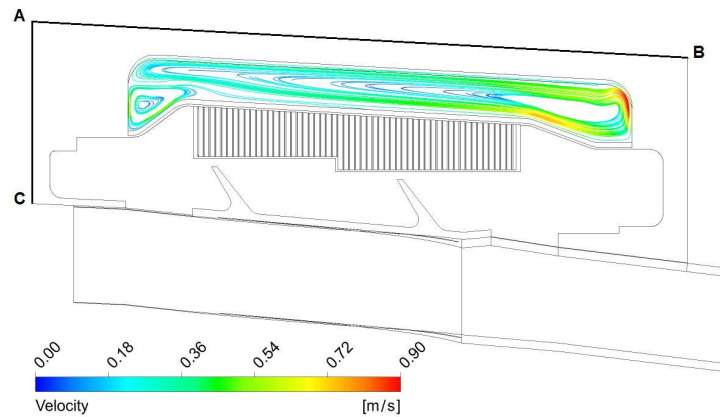


FIG. 11. Streamlines plot in the drum cavity.

tribution; therefore, additional figures with temperature distribution for cases which take radiation into account are not presented. The differences showing the effects of radiation are easier to observe in the charts presented later in this paper.

Figure 11 shows the streamline plot in the cavity. The main vortex is stretched along the whole cavity width. On the left part of the cavity an additional small vortex is created, which fills the gap on the left side of the cavity. The streamlines are coloured according to velocity values in the relative frame of reference. The intensity of air movement in the chamber is low, as indicated by very low speed, not exceeding 1m/s. This is due to the low intensity of heat transfer by convection. A low intensity of convective motions in the cavity can also be observed in Figs. 9 and 10.

The minor importance of the convective motions is caused by the dominant role of the radial temperature distribution. The cooler and denser air is located in the top part of the cavity, so the centrifugal force does not cause movement of gas. The temperature difference in the axial direction is so small that there is no major impact on the movement of air in the cavity. Additionally, the small height of the cavity also plays an important role in limiting the possible convection.

Figure 12 presents the temperature distribution on the outer surface of the casing (line AB in Fig. 11). The maximum temperature difference on the outer wall is calculated at about 120 K for Case I and 90 K for Case II. In cases including radiation (. . . rad) maximum temperature differences are similar. The temperature of the outer surface does not exceed 470 K in Case I, 485 K in Case I rad, 506 K in Case II and 512 K in Case II rad. The average temperature difference resulting from taking radiation into account radiation is about 13.3 K for Case I and 10.6 K for Case II.

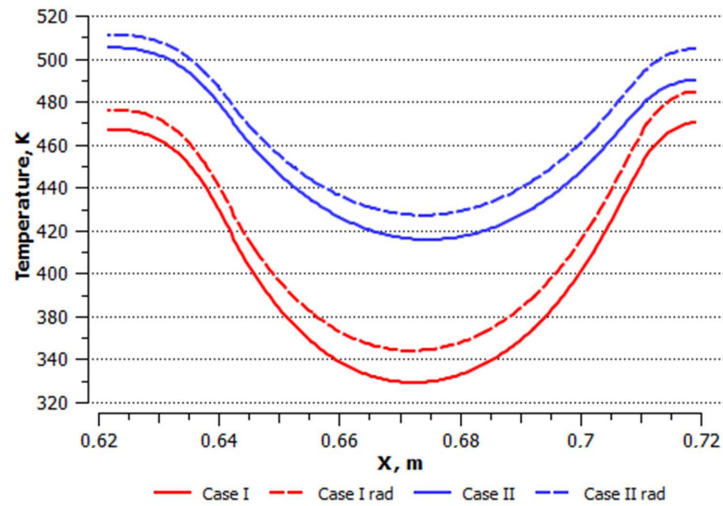


FIG. 12. Temperature distribution in metal along the outer wall.

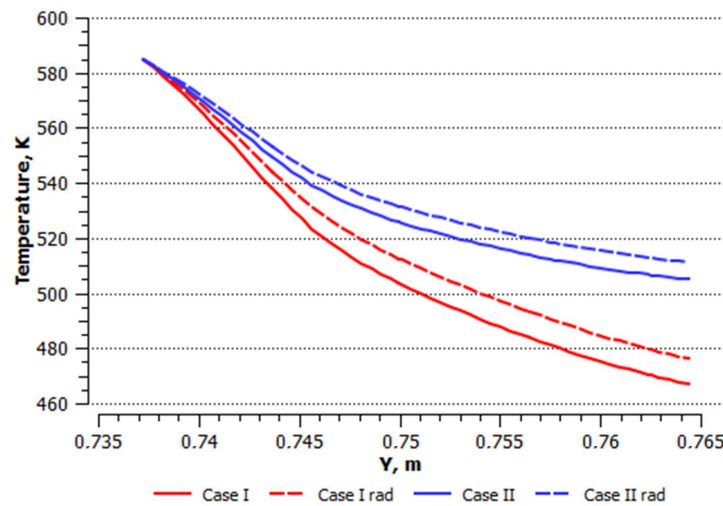


FIG. 13. Temperature distribution in metal in the radial direction.

A similar comparison is presented in Fig. 13, which shows temperature distribution in the radial direction on the left side of the model, on the adiabatic surface (line AC in Fig. 11). For the lowest value of the radius the temperatures are the same, because of the same boundary condition on the bottom surface of the solid. Different values of the heat conductivity coefficient cause that temperatures differ in the remaining part of the surface and this difference increases with the increase of the radius value. The highest difference of about 38 K is at

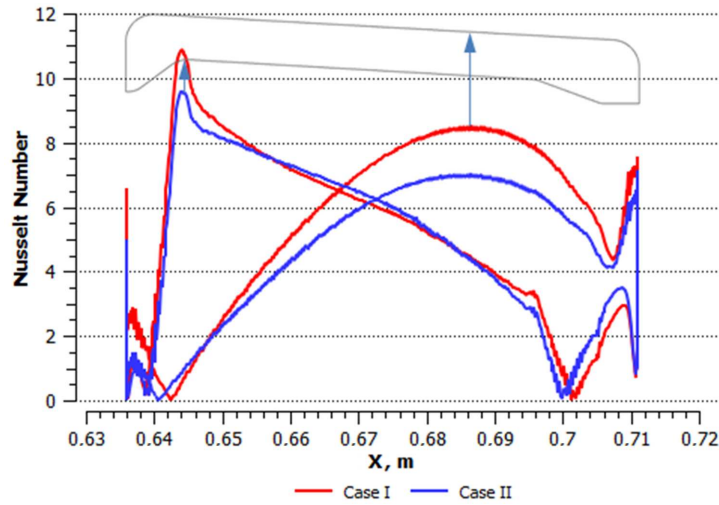


FIG. 14. Nusselt number distribution around the cavity.

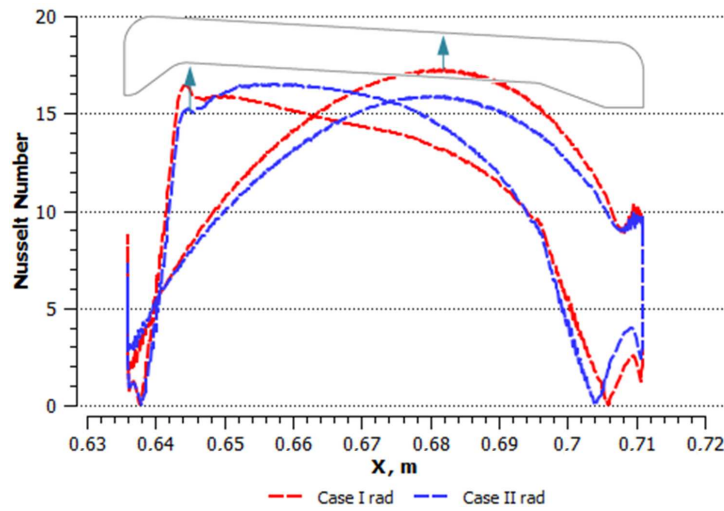


FIG. 15. Nusselt number distribution around the cavity for cases taking radiation into account.

the top of the surface when radiation is neglected and 35 K, when radiation is taken into account.

When analyzing the rotating cavities, a parameter that is often considered is the Nusselt number which is defined in [19] as

$$(4.1) \quad Nu = \frac{q \cdot b/2}{\lambda \cdot \Delta T},$$

where q is the heat flux, b is the cavity width, λ is the thermal conductivity for local temperature and ΔT is the temperature difference. The temperature difference in rotating cavity analysis is generally defined as the difference between the temperature of the heated surface and the inlet temperature of the cooling air for open cavities, and as the temperature difference between the heated and cooled surface for closed cavities. In other words, it is the difference between the highest and lowest temperature in the cavity. The same approach was used in considered case.

For the assumed conditions, the average value of Nusselt number on the cavity walls for Case I was $Nu = 5.28$, whilst for Case II $Nu = 4.75$. For cases taking radiation into account it was 11.21 rad for Case I and 10.99 rad for Case II. So in the cases including radiation the average Nusselt number is more than twice higher than in cases without radiation. The distribution of Nusselt number is presented in Figs. 14 and 15. The highest value of this distribution on the bottom wall of the cavity is located in the area of the arc on the left-hand side of the cavity. On the top surface the maximum value of Nusselt number is located near the right-hand side of the cavity. Information about heat transfer conditions can be useful for conducting more detailed calculations of thermal resistance of the structure.

5. Conclusions

The aim of this study was to examine flow phenomena of the leakage flow through the tip labyrinth seal with honeycomb land in a low-pressure counter-rotating turbine and to perform CHT analysis of the seal area with a part of the casing and the drum cavity.

The calculation domain is relatively large and complex, therefore much attention was given to prepare geometry and mesh. The calculation domain definition method for the rotor blade tip zone was proposed in order to conduct the CHT analysis. The calculations were performed for air ideal gas, where molecular viscosity, thermal conductivity and specific heat at constant pressure were specified as a function of temperature.

The main parameters and flow structures of the leakage flow were described. There are small fluctuations of parameters observed near the honeycomb land, behind fins. The area behind fins is also the place where larger energy dissipation is observed. The other places where the higher energy dissipation was observed are: the inlet chamber, the area near the seal outlet in the outlet chamber and the main flow where mixing takes place.

The flow structures for the cavity and the heat transfer conditions were obtained. The temperature distribution in the whole domain was also considered. A relatively weak forced convection in the cavity was detected, caused by higher

temperature of the inner surface of the cavity, lower of the outer surface and the relatively small radial size of the cavity. The difference of thermal conductivity changes the temperature distribution in the solid, cavity and near the honeycomb.

CHT calculations were performed in two variants, with and without taking radiation into account. Radiation affects the intensification of heat transfer in the upper part of the calculation area, leading to the increase of heat exchange with the surroundings, as demonstrated by the increase of temperature on the outer wall of the casing, on average by 12 K. Temperature differences in the casing elements caused by radiation, however, are much smaller than those resulting from different thermal conductivity coefficient in Cases I and II. Big (more than double) differences appear in the Nusselt number on the cavity walls, what indicates heat exchange much greater than the one resulting from convection.

The determined heat transfer conditions can be used further in strength analyses.

6. Acknowledgements

This work was made possible by the European Union (EU) within the project ACP7-GA-2008-211861 “DREAM” (Validation of **R**adical **E**ngine **A**rchitecture **S**ystems).

The authors would like to thank the Avio Aero for cooperation within the project.

References

1. D. CHERRY, A. WADIA, R. BEACOCK, M. SUBRAMANIAN, P. VITT, *Analytical Investigation of a low pressure turbine with and without flowpath endwall gaps, seals and clearance features*, ASME Paper GT2005-68492, 2005.
2. A.D. VAKILI, A.J. MEGANATHAN, M. MICHAUD, S. RADHAKRISHNAN, *An experimental and numerical study of labyrinth seal flow*, ASME Paper GT2005-68224, 2005.
3. B. ROSIC, J.D. DENTON, *The control of shroud leakage loss by reducing circumferential mixing*, ASME Paper GT2006-90946, 2006.
4. J.E. ANKER, J.F. MAYER, *Simulation of the interaction of labyrinth seal leakage flow and main flow in an axial turbine*, ASME Paper GT2002-30348, 2002.
5. A. GIBONI, K. WOLTER, J.R. MENTER, H. PFOST, *Experimental and numerical investigation into the unsteady interaction of labyrinth seal leakage flow and main flow in a 1.5-stage turbine*, ASME Paper GT2004-53024, 2004.
6. P. ADAMI, F. MARTELLI, S. CECCHI, *Analysis of the shroud leakage flow and main flow interactions in high-pressure turbines using an unsteady CFD approach*, [in:] Proceedings of the European Conference On Turbomachinery ETC2007-165, 2007.

7. B. ROSIC, J.D. DENTON, E.M. CURTIS, A.T. PETERSON, *The influence of shroud and cavity geometry on turbine performance – an experimental and computational study; Part 2: Exit cavity geometry*, ASME Paper GT2007-27770, 2007.
8. R. RUDOLPH, R. SUNSHINE, M. WOODHALL, M. HAENDLER, *Innovative design features of the SGT5-8000h turbine And secondary air system*, ASME Paper GT2009-60137, 2009.
9. J. LI, X. YAN, G. LI, Z. FENG, *Effects of pressure ratio and sealing clearance on leakage flow characteristics in the rotating honeycomb labyrinth*, ASME Paper GT2007-27740, 2007.
10. D.C. CHOI, D.L. RHODE, *Development of a 2-D CFD approach for computing 3-D honeycomb labyrinth leakage*, ASME Paper GT2003-38238, 2003.
11. B.I. SOEMARWOTO, J.C. KOK, K.M.J. DE COCK, A.B. KLOOSTERMAN, G.A. KOOL, *Performance evaluation of gas turbine labyrinth seals using computational fluid dynamics*, ASME Paper GT2007-27905, 2007.
12. H.H. CHOUGULE, D. RAMERTH, D. RAMACHANDRAN, *Low leakage designs for rotor teeth and honeycomb lands in labyrinth seals*, ASME Paper GT2008-51024, 2008.
13. Y. KANG, T.S. KIM, S.Y. KANG, H.K. MOON, *Aerodynamic performance of stepped labyrinth seals for gas turbine applications*, ASME Paper GT2010-23256, 2010.
14. W. WRÓBLEWSKI, S. DYKAS, K. BOCHON, S. RULIK, *Optimization of tip seal with honeycomb land in LP counter rotating gas turbine engine*, *TASK Quarterly*, **14/3**, 189–207, 2010.
15. S. ZECCHI, L. ARCANGELI, B. FACCHINI, *Features of a cooling system simulation tool used in industrial preliminary design stage*, ASME Paper GT2004-53547, 2010.
16. D. BORN, K. HEINIGER, G. ZANAZZI, T. MOKULYS, P. GROSSMANN, L. RIPAMONTI, M. SELL, *Validation of conjugate heat transfer predictions on labyrinth seals and novel designs for improved component lifetime*, ASME Paper GT2011-45358, 2011.
17. K. HE, J. LI, X. YAN, Z. FENG, *Investigations of the conjugate heat transfer and windage effect in stepped labyrinth seals*, *International Journal of Heat and Mass Transfer*, **55**, 4536–4547, 2012.
18. T. WEINBERGER, K. DULLENKOPF, H.-J. BAUER, *Influence of honeycomb facings on the temperature distribution of labyrinth seals*, ASME Paper GT2010-22069, 2010.
19. Z. SUN, K. LINDBLAD, J.W. CHEW, C. YOUNG, *LES and RANS investigations into buoyancy-affected convection in a rotating cavity with a central axial throughflow*, *Transactions of the ASME*, **129**, 318–325, 2007.
20. K. BOCHON, *Numeryczna ocena zjawisk cieplno-przepływowych w wybranych węzłach stopnia turbiny gazowej [in Polish], Numerical investigation of fluid flow and heat transfer phenomena in selected parts of the gas turbine stage – PhD Thesis*, Silesian University of Technology, Gliwice, 2012.

Received October 10, 2014; revised version March 2, 2015.
